Acta Pharmaceutica Sinica B 2017;7(4):496–501

Chinese Pharmaceutical Association
Institute of Materia Medica, Chinese Academy of Medical Sciences

Acta Pharmaceutica Sinica B

www.elsevier.com/locate/apsb
www.sciencedirect.com

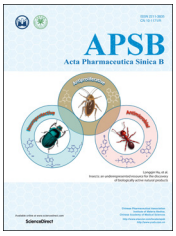

ORIGINAL ARTICLE

Crystal structures, absolute configurations and molecular docking studies of naftopidil enantiomers as α_{1D}-adrenoceptor antagonists

Wei Xu[a], **Junjun Huang**[b], **Renwang Jiang**[a,*], **Mu Yuan**[b,*]

[a]*College of Pharmacy, Jinan University, Guangzhou 510632, China*
[b]*Pharmaceutical Research Center, Guangzhou Medical University, Guangzhou 510182, China*

Received 29 December 2016; received in revised from 28 February 2017; accepted 16 March 2017

KEY WORDS

Naftopidil;
Crystal structure;
α_{1D}-Adrenoceptor antagonists;
Binding mode;
Pharmacophore model

Abstract Chiral drug naftopidil (NAF), a specific α_{1D}-adrenoceptor (AR) antagonist for the treatment of benign prostatic hyperplasia, was used in racemic form for several decades. Our recent work declared that NAF enantiomers showed the same antagonistic effects on the α_{1D}-AR, but the binding mechanism of these two stereochemical NAF isomers to the α_{1D} receptor remained unclear. Herein, we reported the crystallographic structures of optically pure NAF stereoisomers for the first time and unambiguously determined their absolute configurations. The crystal data of *R* and *S* enantiomers matched satisfactorily the pharmacophore model for α_{1D}-selective antagonists. Based on the constructed α_{1D} homology model, molecular docking studies shed light on the molecular mechanism of NAF enantiomers binding to α_{1D}-AR. The results indicated that NAF enantiomers exhibited the very similar binding poses and occupied the same binding pocket.

*Corresponding authors.
E-mail addresses: rwjiang2008@126.com (Renwang Jiang), mryuanmu@aliyun.com (Mu Yuan).

Peer review under responsibility of Institute of Materia Medica, Chinese Academy of Medical Sciences and Chinese Pharmaceutical Association.

http://dx.doi.org/10.1016/j.apsb.2017.04.011

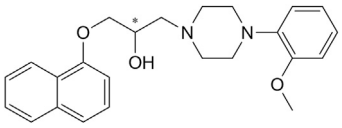

Figure 1 Chemical structure of naftopidil. The asterisk (*) indicates the chiral center.

1. Introduction

Benign prostatic hyperplasia (BPH) is a progressive condition characterized by a nodular enlargement of the prostate resulting in obstruction of the urethra[1]. Emerging contenders to current therapies is focusing on drug targets which are able to relax prostatic smooth muscle in a similar way to the α_1-adrenoceptor (AR) antagonists (α_{1A}-, α_{1B}- and α_{1D}-AR), as this appears to be the most effective mechanism of action[2,3].

Naftopidil (NAF, Fig. 1) is a chiral drug with high selectivity for α_{1A}- and α_{1D}-AR over than for α_{1B} subtype, and exhibits significant clinical efficacy for alleviating lower urinary tract symptoms (LUTS) associated with BPH[4]. However, NAF still remains to be used under racemic form[5]. We also know that the physiochemical and biochemical properties of racemic mixtures and individual stereoisomers can differ significantly. Additionally, stereoselective metabolism of chiral compounds can influence pharmacokinetics, pharmacodynamics, and toxicity. Appropriate chiral antidotes must be selected for therapeutic benefit and to minimize adverse events[6].

Individual NAF enantiomers could be obtained by enantioselective synthesis[7,8] and hydrolytic kinetic resolution[9], but their crystal structures had not been reported so far. We herein described the crystallographic structures of (+)/(–)-NAF and determined their absolute configurations based on single-crystal X-ray diffraction analysis. Moreover, molecular docking studies explored the molecular mechanisms of NAF enantiomers binding to the homology-modeled α_{1D}-AR, which helps to rationally explain their antagonistic activities. This work would provide valuable information for the relationships between stereostructures of chiral molecules and bioactivities.

2. Materials and methods

All reagents and solvents were of analytical grade and commercially available. The ^{1}H NMR spectra were recorded on a Bruker Avance instrument using $CDCl_3$ as a solvent and TMS as an internal standard, and coupling constants (J) were quoted in Hz. Optical rotation measurements were obtained using a Rudolf AUTOPOL IV polarimeter. Single-crystal X-ray diffraction data were collected on a Rigaku RAPID II diffractometer with Cu Kα radiation ($\lambda = 1.54178$ Å).

2.1. Chemistry

(+)/(–)-NAF isomer (ee purity >99.5%) was purchased from Boehringer Mannhei (Ingelheim, Germany). The structure of (+)-NAF was characterized by ^{1}H NMR and high-resolution mass spectrometry (HR-MS). ^{1}H NMR (300 MHz, $CDCl_3$) δ 8.19 (d, $J = 9.3$ Hz, 1H), 7.82 (d, $J = 9.2$ Hz, 1H), 7.57–7.43 (m, 3H), 7.37 (t, $J = 7.9$ Hz, 1H), 7.09 (dd, $J = 10.2$, 6.6 Hz, 1H), 6.91 (t, $J = 7.5$ Hz, 3H), 6.82 (d, $J = 7.6$ Hz, 1H), 5.66 (s, 1H), 4.92 (s, 1H), 4.49–4.30 (m, 1H), 4.24–4.04 (m, 1H), 3.88 (s, 5H), 3.54 (s, 4H), 3.46 (d, $J = 8.1$ Hz, 2H), 3.28 (d, $J = 15.8$ Hz, 2H). HR-MS (ESI) m/z Calcd. for $C_{24}H_{28}N_2O_3$ $[M + H]^+$, 393.2100; Found, 393.2104.

2.2. X-ray crystallography

Suitable crystals of NAF enantiomers were obtained by slowly evaporating a mixture of dichloromethane and n-hexane solution at ambient temperature. High-quality colorless crystals were mounted on a glass fiber in a random orientation. The data were collected by an R-AXIS RAPID II diffractometer equipped with graphite-monochromatic Cu Kα radiation ($\lambda = 1.54178$ Å) by using the ω scan mode. The structures were solved by direct methods using Olex2 software[10], and the non-hydrogen atoms were located from the trial structure[11] and then refined anisotropically with SHELXL

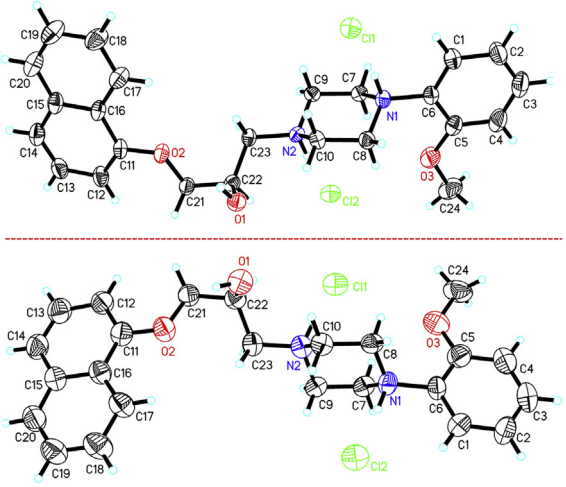

Figure 2 Crystallographic structures of (*R*)-(+)-NAF · 2(HCl) (upper) and (*S*)-(–)-NAF · 2(HCl) (lower). Displacement ellipsoids are drawn at the 30% probability level.

Table 1 Crystal data and structural refinement of compounds (*R*)-(+)-NAF · 2(HCl) and (*S*)-(–)-NAF · 2(HCl).

Compd.	(*R*)-(+)-NAF · 2(HCl)	(*S*)-(–)-NAF · 2(HCl)
Chemical formula	$C_{24}H_{28}N_2O_3 \cdot 2(HCl)$	$C_{24}H_{28}N_2O_3 \cdot 2(HCl)$
MW	465.40	465.40
Crystal system, space group	Monoclinic, $P2_1$	Monoclinic, $P2_1$
a, b, c (Å)	11.777(2), 5.7595(12), 17.464(4)	11.776(2), 5.7561(12), 17.462(4)
α, β, γ (°)	90, 95.03(3), 90	90, 95.02(3), 90
V (Å^3)	1180.0(4)	1179.1(4)
Z	2	2
ρ_{calc} (g/cm^3)	1.310	1.311
μ (mm^{-1})	2.697	2.700
F (000)	492.0	492.0
Crystal size (mm^3)	0.3 × 0.2 × 0.2	0.3 × 0.2 × 0.2
Radiation	Cu Kα (λ=1.54178)	Cu Kα (λ=1.54178)
θ range (°)	3.767 to 68.212	3.768 to 68.220
T_{min}/T_{max}	0.550/0.583	0.549/0.583
Reflections collected/unique/observed	19516/3984/2759	21209/4089/1825
Goodness-of-fit on F^2	1.119	1.181
R_1/wR_2 [$I \geq 2\sigma$ (I)]	0.0552/0.1203	0.1085/0.2593
$\Delta\rho_{max}/\Delta\rho_{min}$ (e Å^{-3})	0.49/–0.28	0.54/–0.40
Flack/Hooft parameters	0.012(14)/0.022(14)	0.04(2)/0.086(17)

using a full-matrix least squares procedure based on F^2. The weighted R factor, wR and goodness-of-fit S values were obtained based on F^2. The hydrogen atom positions were fixed geometrically at the calculated distances and allowed to ride on the parent atoms. Crystallographic data excluding structure factors have been deposited at the Cambridge Crystallographic Data Center (CCDC). CCDC 1023461 contains the supplementary crystallographic data for this paper.

2.3. *Homology modeling and molecular docking*

The amino acidic sequences of the human α_{1D} receptor were retrieved from SwissProt database (entry code: P25100, ADA1D_HUMAN).

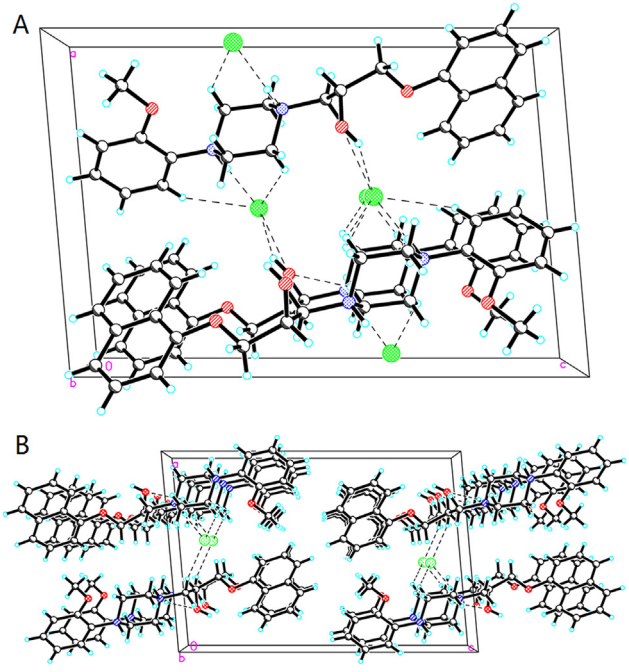

Figure 3 Crystal packing of (*R*)-NAF · 2(HCl) (A) and (*S*)-NAF · 2(HCl) (B) along the *b* axis. Black dashed lines show the intermolecular H-bonds.

The homology model of α_{1D} subtype was successfully produced by our previous work[12], and then submitted to be energy optimization by using CHARMMing program. Structural evaluation and stereochemical analyses were performed using PROCHECK, PROVE, CRYST and Ramchandran plot[13]. PyMOL software was employed for checking and validating protein structures after model refinement.

The crystallographic structures of NAF enantiomers were saved in mol2 format. The preparation of the pdbqt files was done by standard procedure using AutoDock Tools 1.4.6[14]. The docking procedures were performed in AutoDock Vina using the default scorning function[15]. The binding site was identified according to previous studies[16]. Exhaustiveness was set to 100, and number of output conformations was set to 20. The searching seed was random. The calculated geometries were ranked in terms of free energy of binding and the best poses were selected for further analysis.

3. Results and discussion

3.1. *Crystal structures of NAF enantiomers*

(+)/(–)-NAF were converted to their hydrochloride salts, *i.e.*, NAF · 2(HCl), with $[\alpha]_D^{25}$ +23.7° (*c* 0.439, CH_3OH) and –24.0° (*c* 0.481, CH_3OH), respectively. Both enantiomers (+)-NAF · 2(HCl) and (–)-NAF · 2(HCl) crystallized in the monoclinic space group $P2_1$ with one crystallographically independent molecule in the asymmetric unit. Their representative crystal structures are presented in Fig. 2 and exhibit good mirror symmetry. Crystal data and structural refinement are shown in Table 1.

The dihedral angle between benzene ring and naphthalene plane was 18.0(3)° for (+)-NAF and 18.1(5)° for (–)-NAF, respectively. The piperazine ring indicated a chair-type geometry. Interestingly, intermolecular H-bonds (O–H · · · Cl, N–H · · · Cl and C–H · · · Cl, Fig. 3 and Table 2) played critical roles in stabilizing the packing structures. In addition, NAF in the crystal was assembled in a way to yield a high density (1.310 g/cm^3), in which one and/or two overlapping molecules were regularly arranged and were thought to be kept in balance by intermolecular van der Waals forces[17].

Table 2 Intermolecular hydrogen bonds for compounds (+)/(–)-NAF · 2(HCl) (Å, °).

D—H · · · A	D—H	H · · · A	D · · · A	D—H · · · A (°)
(+)-NAF · 2(HCl)				
O(1)—H(1) · · · Cl(1)[a]	0.82	2.44	3.1767(7)	151
N(2)—H(2) · · · Cl(2)[b]	0.98	2.04	3.0016(6)	168
C(10)—H(10B) · · · Cl(1)[c]	0.97	2.72	3.4258(7)	130
(–)-NAF · 2(HCl)				
N(1)—H(1 A) · · · Cl(2)[d]	0.98	2.00	2.9686(7)	172
O(1)—H(1B) · · · Cl(2)[e]	0.82	2.72	3.1788(7)	117
C(10)—H(10B) · · · Cl(2)[f]	0.97	2.71	3.4208(8)	130

Symmetry code: [a] $x,-1+y,z$; [b] $1-x,-1/2+y,1-z$; [c] $1-x,1/2+y,1-z$; [d] $1+x,y,z$; [e] $1-x,-1/2+y,-z$; [f] $1+x,-1+y,z$.

We could determine the absolute structure of (+)-NAF · 2(HCl) based on the calculated Flack parameter[18] 0.012(14). The Hooft parameter[19] of 0.022(14) was also sufficient to confirm the absolute structure. The absolute configuration of the chiral center of (+)-NAF · 2(HCl) was thus determined to be *R*. Similarly, (–)-NAF · 2(HCl) was also unambiguously assigned to be *S* since the small Flack and Hooft parameters 0.04(2) and 0.086(17), respectively.

Interestingly, crystal data of NAF enantiomers were satisfied with the pharmacophoric model for selective α_{1D}-AR antagonists (Table 3). It can be seen that the measured distances of PI-HY1 (5.6 Å) and PI-HBA (4.2 Å) were nearly equal to that of the α_{1D} model.

3.2. *Molecular docking studies*

(*R*)-NAF, (*S*)-NAF and racemic NAF showed similar α_{1D}-AR antagonistic effects with the pA_2 values of 7.85, 8.03 and 7.93, respectively[20]. Although (*R*)- and (*S*)-NAF exhibited the same high affinity towards α_{1D}-AR, the binding mechanisms of NAF enantiomers to the α_{1D} receptor were still unclear. Then molecular docking analysis was performed, which might shed light on the antagonistic properties of NAF enantiomers over α_{1D}-AR.

Table 3 Visualization of pharmacophoric features of NAF based on Barbaro's model and comparison of important distances between pharmacophoric features in reported subtype-selective α_1-AR antagonists and crystallographic structures of NAF enantiomers. Colour legend: green, hydrophobic features (HY); blue, positive ionizable (PI); rose, hydrogen bond donor (HBD); red, hydrogen bond acceptor (HBA).

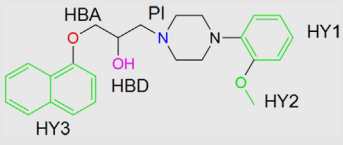

X-ray structure	Distance (Å)			
	PI-HY1	PI-HBA	PI-HY3	PI-HBD
α_{1A}-AR antagonists	5.5	7.1	–	–
α_{1B}-AR antagonists	6.2	–	7.8	4.9
α_{1D}-AR antagonists	5.4	4.5	–	–
(*R*)-NAF	5.6	4.2	6.8	3.1
(*S*)-NAF	5.6	4.2	6.9	3.1

– Not applicable.

α_{1D}-AR is a member of the G protein–coupled receptors (GPCRs) family that are constructed by seven transmembrane (TM) helices, N- and C-terminal fragments, and intra- and extracellular loop (ECL) regions[21,22]. Molecular docking was performed on α_{1D} receptor constructed by homology model building using the AutoDock-vina program since the accurate 3D structures of α_{1D}-AR with high resolutions has not been obtained yet[12]. To achieve the reliable docking results, the lowest energy conformations of NAF enantiomers were extracted from their crystal structures and the α_{1D}-AR model was submitted to be energy optimization by using CHARMMing program. The top ranked poses of (*R*)-NAF and (*S*)-NAF (Fig. 4A and B) both positioned in the hydrophobic pocket involving TM 2, 3, 6 and 7 with the same calculated binding energies (–9.0 kcal/mol). The OH group of (*R*)-NAF formed a hydrogen bond (2.6 Å) with Glu190 in the ECL2 region that has been reported to be essential for GPCR activation[23]. The methoxyl at the arylpiperazine moiety formed an H-bond with Thr189 (3.0 Å between the oxygen atom of methoxyl group and the hydroxyl oxygen atom of Thr189). The protonated piperazine moiety formed an electrostatic interaction (3.1 Å) with Thr189 of ECL2, and the benzene ring was mainly engaged in hydrophobic interactions with Phe185 and Trp175 residues. Additionally, the naphthalene moiety was placed in the hydrophobic region among TM5, TM6 and TM7, and contacted *via* hydrophobic interactions with residues Phe304, Phe305 and Phe324. As compared to the binding mode for (*R*)-NAF-α_{1D} complex, (*S*)-NAF showed very similar binding behavior (Fig. 3B). On the basis of the similar binding poses and binding energies of (*R*)/(*S*)-NAF with α_{1D} receptor, we can rationally explain the similar antagonistic activities towards α_{1D}. On the other hand, it indicated that the α_{1D} homology model was feasible and useful for virtual screening of the α_{1D}-selective blockers. Furthermore, we inferred that residues Glu190 and Thr189 played an important role in recognizing the α_{1D} subtype, especially for arylpiperazine-based antagonists.

4. Conclusions

In this work, we reported the crystallographic structures of NFA enantiomers for the first time, and unambiguously determined their absolute configurations based on the Flack and Hooft

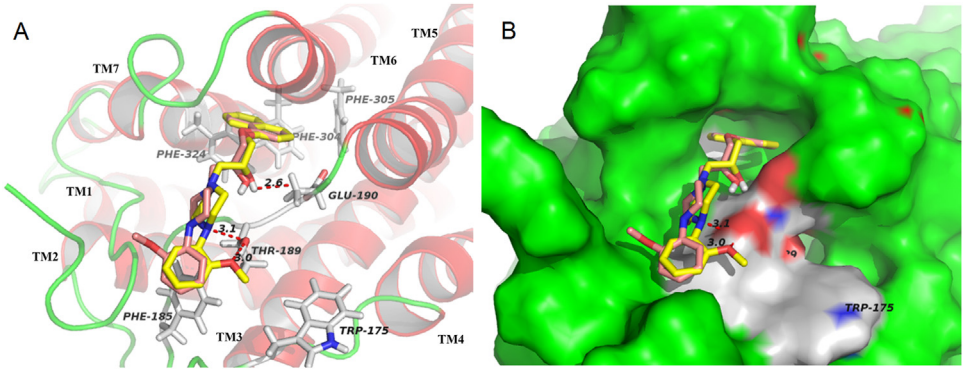

Figure 4 (A) The top-ranked docking poses of (*R*)-NAF (yellow carbons) and (*S*)-NAF (magenta carbons) into the putative binding sites of α_{1D}-AR. (B) α_{1D} (surface)–ligand (stick) complex. The two antagonists are shown in stick representation. The receptors are shown in cartoon representation with red alpha helices and green loops. The seven TM helices are labeled by 1, 2, 3, 4, 5, 6 and 7, respectively. Dashed lines represent the hydrogen bonds or electrostatic interactions.

parameters. In crystal packing, specific intermolecular hydrogen bonds [O–H · · · Cl, N–H · · · Cl and C–H · · · Cl] are found to stabilize the three-dimensional structure. Furthermore, NAF enantiomers fitted well with the ligand-based pharmacophore model for α_{1D}-selective antagonists.

(*R*)- and (*S*)-NAF exhibited the similar antagonistic activities towards α_{1D}-AR, but the underlying mechanisms still remain unclear. Molecular docking studies revealed the binding modes of NAF enantiomers to the α_{1D} receptor associated with their antagonistic effects. Docking results indicated that the OH group *via* H-bond contacted with Glu190 in the ECL2, which might play an important role in the recognition of α_{1D}-AR. The arylpiperazine part was placed on the entrance of hydrophobic pocket, and the naphthalene moiety entered into a deep hydrophobic region surrounded by TM 5, 6 and 7. Binding mode of (*R*)-NAF was very similar to that of (*S*)-NAF, which was consistent with our previous report that the enantiomers had the same antagonistic potency for α_{1D}-AR. Details of NAF enantiomers binding mode provide valuable clues for the design of selective α_{1D}-AR antagonists in the future.

Acknowledgments

This work was supported by grants from the National Science Foundation of Guangdong Province (No. S2013040014088), the Postdoctoral Science Foundation of Guangzhou City (Q188) and partially supported by the Guangdong Major Scientific and Technological Special Project for New Drug Development (2013A022100029).

References

1. Sarswat A, Kumar R, Kumar L, Lal N, Sharma S, Prabhakar YS, et al. Arylpiperazines for management of benign prostatic hyperplasia: design, synthesis, quantitative structure–activity relationships, and pharmacokinetic studies. *J Med Chem* 2011;**54**:302–11.
2. Meyer MD, Altenbach RJ, Basha FZ, Carroll WA, Condon S, Elmore SW, et al. Structure-activity studies for a novel series of tricyclic substituted hexahydrobenz[*e*]isoindole α_{1A} adrenoceptor antagonists as potential agents for the symptomatic treatment of benign prostatic hyperplasia (BPH). *J Med Chem* 2000;**43**:1586–603.
3. Ventura S, Oliver VL, White CW, Xie JH, Haynes JM, Exintaris B. Novel drug targets for the pharmacotherapy of benign prostatic hyperplasia (BPH). *Br J Pharmacol* 2011;**163**:891–907.
4. Castiglione F, Benigni F, Briganti A, Salonia A, Villa L, Nini A, et al. Naftopidil for the treatment of benign prostate hyperplasia: a systematic review. *Curr Med Res Opin* 2014;**30**:719–32.
5. Hara N, Mizusawa T, Obara K, Takahashi K. The role of naftopidil in the management of benign prostatic hyperplasia. *Ther Adv Urol* 2013;**5**:111–9.
6. Smith SW. Chiral toxicology: it's the same thing…only different. *Toxicol Sci* 2009;**110**:4–30.
7. Pujala B, Chakraborti AK. Zinc(II) perchlorate hexahydrate catalyzed opening of epoxide ring by amines: applications to synthesis of (*RS*)/(*R*)-propranolols and (*RS*)/(*R*)/(*S*)-naftopidils. *J Org Chem* 2007;**72**:3713–22.
8. Panchgalle SP, Gore RG, Chavan SP, Kalkote UR. Organocatalytic enantioselective synthesis of *β*-blockers: (*S*)-propranolol and (*S*)-naftopidil. *Tetrahedron: Asymmetry* 2009;**20**:1767–70.
9. Kiran KK, Subhas BD. The first enantiomerically pure synthesis of (*S*)-and (*R*)-naftopidil utilizing hydrolytic kinetic resolution of (±)-(*α*-naphthyl) glycidyl ether. *Chem Lett* 2004;**33**:1212–3.
10. Dolomanov OV, Bourhis LJ, Gildea RJ, Howard JA, Puschmann H. *OLEX2*: a complete structure solution, refinement and analysis program. *J Appl Cryst* 2009;**42**:339–41.
11. Kratzert D, Holstein JJ, Krossing I. DSR: enhanced modelling and refinement of disordered structures with SHELXL. *J Appl Cryst* 2015;**48**:933–8.
12. Xu W, Huang J, Shao B, Xu X, Jiang R, Yuan M. Design, synthesis, crystal structure, biological evaluation and molecular docking studies of carbazole-arylpiperazine derivatives. *Bioorg Med Chem* 2016;**24**:5565–72.
13. Sashidhara KV, Avula SR, Doharey PK, Singh LR, Balaramnavar VM, Gupta J, et al. Designing, synthesis of selective and high-affinity chalcone-benzothiazole hybrids as *Brugia malayi* thymidylate kinase inhibitors: *in vitro* validation and docking studies. *Eur J Med Chem* 2015;**103**:418–28.
14. Morris GM, Huey R, Lindstrom W, Sanner MF, Belew RK, Goodsell DS, et al. AutoDock4 and AutoDockTools4: automated docking with selective receptor flexibility. *J Comput Chem* 2009;**30**:2785–91.
15. Trott O, Olson AJ. AutoDock Vina: improving the speed and accuracy of docking with a new scoring function, efficient optimization, and multithreading. *J Comput Chem* 2010;**31**:455–61.
16. Xu W, Shao B, Xu X, Yuan M, Yuan M. Structural analysis of (*S*)-1-((1*H*-benzo[*d*][1,2,3]triazol-1-yl)oxy)-3-(4-(2-methoxyphenyl)piperazin-1-yl)propan-2-ol and binding mechanism with α_{1A}-adrenoceptor: tddft calculations, X-ray crystallography and molecular docking. *J Mol Struct* 2016;**1106**:485–90.
17. Xu JB, Zhang H, Gan LS, Han YS, Wainberg MA, Yue JM. Logeracemin A, an anti-HIV *Daphniphyllum* alkaloid dimer with a

new carbon skeleton from *Daphniphyllum longeracemosum*. *J Am Chem Soc* 2014;**136**:7631–3.
18. Flack HD, Bernardinelli G. The use of X-ray crystallography to determine absolute configuration. *Chirality* 2008;**20**:681–90.
19. Hooft RW, Straver LH, Spek AL. Determination of absolute structure using Bayesian statistics on Bijvoet differences. *J Appl Cryst* 2008;**41**:96–103.
20. Huang JJ, Cai Y, Yi YZ, Huang MY, Zhu L, He F, et al. Pharmaceutical evaluation of naftopidil enantiomers: rat functional assays *in vitro* and estrogen/androgen induced rat benign prostatic hyperplasia model *in vivo*. *Eur J Pharmacol* 2016;**791**:473–81.
21. Pedretti A, Silva ME, Villa L, Vistoli G. Binding site analysis of full-length α_{1a} adrenergic receptor using homology modeling and molecular docking. *Biochem Biophys Res Commun* 2004 493–500.
22. Goldfeld DA, Zhu K, Beuming T, Friesner RA. Successful prediction of the intra-and extracellular loops of four G-protein-coupled receptors. *Proc Natl Acad Sci U S A* 2011;**108**:8275–80.
23. Zhao XF, Wang J, Liu GX, Fan TP, Zhang YJ, Yu J, et al. Binding mechanism of nine *N*-phenylpiperazine derivatives and α_{1A}-adrenoceptor using site-directed molecular docking and high performance affinity chromatography. *RSC Adv* 2015;**5**:57050–7.